Applied Physics Letters ARTICLE scitation.org/journal/apl

Na_2FeF_4 as a stable cathode material for Na-ion batteries

Cite as: Appl. Phys. Lett. **121**, 143902 (2022); doi: 10.1063/5.0111765
Submitted: 19 July 2022 · Accepted: 12 September 2022 ·
Published Online: 3 October 2022

Qi Yan,[1,2] Huan Xu,[1,3] Khang Hoang,[4] Xiaolong Zhou,[1] Pinit Kidkhunthod,[5] Philip Lightfoot,[6] Wenjiao Yao,[1,7,a)] and Yongbing Tang[1,3,8,a)]

AFFILIATIONS

[1]Advanced Energy Storage Technology Research Center, Shenzhen Institutes of Advanced Technology, Chinese Academy of Sciences, Shenzhen 518055, China
[2]Nano Science and Technology Institute, University of Science and Technology of China, Suzhou 215123, China
[3]School of Chemical Sciences, University of Chinese Academy of Sciences, Shenzhen 518055, China
[4]Center for Computationally Assisted Science and Technology and Department of Physics, North Dakota State University, Fargo, North Dakota 58108, USA
[5]Synchrotron Light Research Institute, Nakhon Ratchasima 30000, Thailand
[6]School of Chemistry and EaStChem, University of St Andrews, St Andrews, Fife KY16 9ST, United Kingdom
[7]Shenzhen Key Laboratory of Energy Materials for Carbon Neutrality, Shenzhen 518055, China
[8]Key Laboratory of Advanced Materials Processing & Mold, Ministry of Education, Zhengzhou University, Zhengzhou 450002, China

Note: This paper is part of the APL Special Collection on New Technologies and New Applications of Advanced Batteries.
[a)]**Authors to whom correspondence should be addressed:** wj.yao@siat.ac.cn and tangyb@siat.ac.cn

ABSTRACT

In the search of cathode materials for Na-ion batteries, iron-based compounds have attracted much attention due to the abundant resource, easy access, and environmental friendliness of iron. Herein, we report the synthesis, structure, and electrochemistry of a previously unknown compound in the Na–Fe–F system, formulated as Na_2FeF_4. It is prepared by an easy and mild hydrothermal reaction with oxalate as a Fe^{2+} protector. Based on the single crystal x-ray diffraction analysis, it crystallizes in space group *Pmcb* with $a = 3.255$ (3) Å, $b = 5.591(7)$ Å, and $c = 9.557(1)$ Å. The crystal structure features edge-sharing FeF_6 octahedra to form $[FeF_4]_\infty$ chains with Na^+ ions located between chains. In electrochemical investigations, it is demonstrated that the material can deliver a reversible capacity of ~90 mAh g^{-1} for 300 cycles in the window of 1.5–4.3 V with redox reactions at ~3.0 V (vs Na^+/Na). Such an activity originates from the Fe^{3+}/Fe^{2+} redox couple, confirmed by x-ray absorption spectra and first-principles calculations.

Inorganic metal halides are of great importance in developing materials for energy production and storage, microelectronics and photonics, photoluminescence, catalysis, automotive applications, etc.[1,2] Among these, alkali metal–transition metal fluoride compounds ($A_xM_yF_z$, A/M either single or mixed atoms) are gaining increasing attention for their potential applications in magnetism, multiferroicity, and ion conductivity as well as electrochemistry.[3,4] Being a basic task for solid state chemists, profound studies have been carried out to gain better knowledge of relationships between the structure and pertinent physical properties. As expected, the diverse properties of $A_xM_yF_z$ compounds may be attributed intrinsically to their diverse structural types. Usually, the structure of $A_xM_yF_z$ fluorides is described by the connectivity of the $(MF_n)^{m-}$ building units, when these polyhedra share one, two, or three vertices to form isolated polyanions, chains, layers, or three-dimensional $[M_yF_z]^{x-}$ frameworks. Several families, including AMF_3, AMF_4, A_2MF_5, A_2MF_6, A_3MF_6, and $A_2M_2F_7$, are well characterized.[5]

At the same time, with the critical role of sodium-ion batteries for large scale energy storage,[6–9] iron-based compounds have gained much attention as potential cathode materials, especially for Fe^{2+}-based ones, which show merits of rich resources, easy access, and environmental friendliness.[10–12] Therefore, intensive efforts have been devoted to the $Na_xFe_yF_z$ system, resulting in the discovery of $NaFeF_3$, $NaFeF_4$, $Na_2Fe_2F_7$, Na_3FeF_6, and $Na_5Fe_3F_{14}$.[13–18] The applied synthesis techniques include conventional solid-state reactions and unconventional processes such as solvothermal, mechanochemical, gaseous

fluorination, and reaction in ionic liquids.[13,14,19] Since iron exhibits variable oxidation states, explicit control of synthesis conditions is required to obtain the desired target. In solvothermal methods, an HF solution is widely used as a fluorine source. However, it is a contact-poison with the potential for deep, initially painless burns or even worse damage to humans. Therefore, caution should be taken to avoid any skin exposure. Moreover, in mechanochemical methods, a protective atmosphere, such as Ar gas, is needed to keep iron in the reduced state, Fe^{2+}.

Herein, we present an easy and mild method to stabilize Fe^{2+}, and we report the discovery of an unknown compound in the Na–Fe–F ternary system formulated as Na_2FeF_4. Determined from single crystal x-ray diffraction data, its structure is characterized by parallel-aligned $[FeF_4]_\infty$ chains composed of edge-shared FeF_6 octahedra with sodium ions locating between the chains. Moreover, its electrochemical performance is thoroughly studied as a cathode material in a Na-ion battery. It exhibits a reversible capacity of ~90 mAh g^{-1} with redox reactions at ~3.0 V vs Na^+/Na in the window of 1.5–4.3 V for 300 cycles. Such an activity originates from the Fe^{3+}/Fe^{2+} redox couple, as confirmed by x-ray absorption spectra and first principles calculations.

We have recently shown that solvothermal synthesis is a good way of crystallizing molecular-based magnetic materials, particularly when small anions, such as oxalate and squarate, are used.[20,21] This approach has several advantages, including the ability to synthesize otherwise unobtainable materials and the possibility to form materials in which the structure is modified by the presence of included small ions such as halides and groups 1 and 2 cations, within the lattice. In this work, using oxalate acid as both the pH adjustor and Fe^{2+} protector, light yellow transparent Na_2FeF_4 crystallites [Fig. 1(a)] were synthesized by a hydrothermal reaction. The chemical composition of a crystallite was determined by energy dispersive x-ray spectroscopy (EDS) coupled with scanning electron microscopy (SEM) (Fig. S1 and Table S1 in the supplementary material). Since the analytical data on composition from EDS are only qualitative, often with high errors, a single crystal was chosen to collect single crystal x-ray diffraction data (SXRD), which is a sound technique to detect the accurate composition as well as the structure of crystalline samples. Based on the SXRD, the chemical formula of the obtained sample is Na_2FeF_4, and it adopts the Sr_2PbO_4 structure type in the orthorhombic space group *Pmcb* (no. 55) with one iron, one sodium, and two independent fluorine sites in each asymmetric unit (Tables S2 and S3 in the supplementary material). The structure consists of infinite edge-sharing chains of FeF_6 octahedra propagating along the *a*-axis [Figs. 1(b) and 1(c)] with Na in "capped" trigonal prismatic (seven-coordinate) sites between chains (Fig. S2 in the supplementary material). The Fe atom sits on a site of 2/*m* point symmetry, leading to four equivalent, bridging Fe–F bonds of 1.993 Å and two shorter terminal Fe–F bonds of 2.217 Å (Fig. S3 and Table S4 in the supplementary material). The orthorhombic Sr_2PbO_4 structure type is structurally related to the high pressure "post-perovskite" phase of $MgSiO_3$, in which the edge-sharing chains are further linked through shared octahedral corners into infinite sheets.[22]

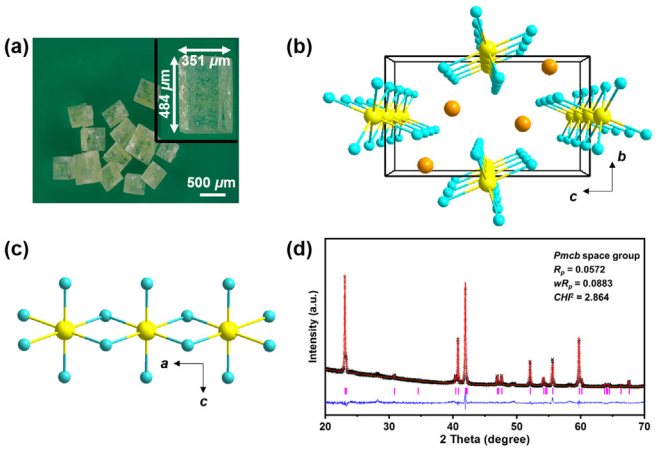

FIG. 1. Characterization and structure analysis of Na_2FeF_4. (a) The optical micrograph. (b) Unit cell showing parallel-aligned $[FeF_4]_\infty$ chains. (c) A $[FeF_4]_\infty$ chain. (d) Rietveld refinement of the PXRD pattern.

Further analogs of Na_2FeF_4 are known for chlorides, Na_2MCl_4 (M = Mn, Mg, Cd), but this exact structure type has not previously been reported for a fluoride.[23] There is, however, a monoclinic variant, which occurs for Jahn–Teller active M, for example, in Na_2CrCl_4, Na_2CuF_4, Na_2CrF_4, Na_2AgF_4, and β-K_2AgF_4. The elongation of the MX_6 octahedron due to the Jahn–Teller effect lowers the site symmetry at M to $\bar{1}$, leading to three distinct M–X bonds and space group $P2_1/c$ (Table S5 in the supplementary material).

The existence of two polymorphs of K_2AgF_4 illustrates the subtle balance between different competing polymorphs of stoichiometry A_2BX_4. In the case of the fluorides, the well-known layered perovskite (Ruddlesden–Popper) type K_2NiF_4 structure and its lower symmetry variants are favored for larger A-cations (A = K, Rb, or Cs), and this is indeed the structural family of the metastable α-K_2AgF_4 in addition to K_2FeF_4 and Rb_2FeF_4.[24] The Li-containing fluorides and chlorides, A_2BX_4, prefer the inverse spinel structure type with both octahedral and tetrahedral Li. Other known phases in the Na–Fe^{II}–F system include both the perovskite and post-perovskite polymorphs of $NaFeF_3$.

A powder x-ray diffraction (PXRD) pattern on a hand-ground sample was collected, and the Rietveld method was used to fit the data to the single crystal structural model. The result shows that the phase of the powder agrees well with the single crystal structure and is of high purity [Fig. 1(d)]. The infrared (IR) spectrum shows only three absorption peaks at small wavenumbers, i.e., 455, 436, and 413 cm^{-1} (Fig. S4 in the supplementary material), which can be assigned to Fe–F vibrations.[25] It further confirms the sample's composition.

Air stability is also an important consideration for electrode materials. Materials with good air stability can avoid the complexity of preparation and storage processes, which may otherwise cause composition and structure changes and, thus, performance degradation. Meanwhile, the easy storage conditions can also reduce the cost. To evaluate the air stability of Na_2FeF_4, its crystallites were placed on plastic petri dishes and exposed to air (room temperature, about 60% humidity). The Na_2FeF_4 crystallites before and after air exposure were characterized by optical microscopy, PXRD, and FTIR. After 7 and 14 days of air exposure, trace amounts of black impurities appeared on the surface, while no other observable crystal defects (cracking, pulverization, water absorption) can be seen [Figs. S5(a)–S5(c) in the supplementary material]. The PXRD and FTIR spectra of the original

samples were compared with those exposed to air for 7 and 14 days, and these were basically the same [Figs. S5(d) and S5(e) in the supplementary material]. Therefore, it can be concluded that Na_2FeF_4 has good air stability.

Supposing the Fe^{2+}/Fe^{3+} redox couple works out in Na_2FeF_4 as in most iron-based cathode materials, its theoretical specific capacity is calculated to be ~150 mA g^{-1}. Meanwhile, if the valence state of iron goes further to +4, which has been reported in a few cases, a theoretical capacity as high as 300 mA g^{-1} can be expected.

Before the electrochemical study, pristine crystallites were ball-milled and mixed with conductive carbon to improve the sample's electric conductivity. Samples after each treatment were checked by PXRD to ensure their phase purity [Fig. S6(a) in the supplementary material]. The broadened diffraction peaks after ball milling also indicate the particles have been downsized significantly. The final composite powder was checked by SEM and EDS [Fig. S6(b) in the supplementary material], which showed the particles of Na_2FeF_4 had been reduced to micrometer size, on average, and are evenly mixed with conductive carbon. Such a composite is thereafter coated on carbon-coated aluminum foils and ready to serve as an electrode.

The electrochemical activity of Na_2FeF_4 was tested in a galvanostatic mode. As the iron in the pristine sample is in the +2 valence state, the test started from charging. Figure 2(a) presents a typical stabilized galvanostatic charge–discharge (GCD) curve of a Na-half cell in the voltage window of 1.5–4.3 V at the current density of 0.1 C (1 C = 150 mA g^{-1}, details in Methods in the supplementary material). Two related plateaus can be observed at 3.05 and 2.97 V for the charge and discharge processes, respectively [Fig. 2(b)]. The initial cycles (~25) are activating processes, after which the cell is stabilized with a discharging capacity of approximately 90 mAh g^{-1} (based on the weight of Na_2FeF_4) and Coulombic efficiency (CE) approaching 99.8% [Figs. 2(c) and 2(d)]. The plateaus became more obvious along with cycles, thanks to the more exposed active sites upon electrochemical grinding effect. After 300 cycles, the discharging capacity remains 90 mAh g^{-1}. The cell exhibits excellent stability as can be clearly seen from the time-dependent cycling curves and the average discharge voltage for the last 50 cycles (Fig. S7 in the supplementary material).

The rate performance is also evaluated by changing the current density [Fig. 2(e)]. From 0.05, 0.1, 0.5, 1, 2 to 3 C, the cell's capacity drops down gradually from 107 to 48 mAh g^{-1}. The capacity retention from 0.05 to 3 C is around 45%. Afterwards, with the decrease in the current density, the capacity increases step by step and returns to 100 mAh g^{-1} at 0.05 C. The CE for each current density is generally steady at 95%. Such results demonstrate the stability and also the good rate performance of the Na_2FeF_4 cathode compared with other fluoride cathodes (Table S6 in the supplementary material).

As a supplementary study, the capability of Li-ion storage in the Na_2FeF_4 cathode was preliminarily measured using a Li foil anode and a Li-ion electrolyte. Lithium and sodium are analogous to each other, while their radii are different, i.e., 0.76 and 1.02 Å for Li^+ and Na^+, respectively. Normally, materials capable of Na^+ storage are also suitable for Li^+ storage, but the opposite shall depend on more factors such as channel size and framework stability. The radius difference also causes the easier and faster Li^+ migration than Na^+ in the host materials. Therefore, the Na^+ ions desert from the Na_2FeF_4 cathode in the initial charging process, and then Li^+ ions from the electrolyte insert in the cathode in the initial discharging process. The following cycles shall work on Li^+ de-/insertion. Similar phenomenon has also been reported widely.[26,27] Our cells cycled in the 1.5–4.3 and 2.0–4.3 V displayed similar redox reactions above 3.0 V after stabilization,

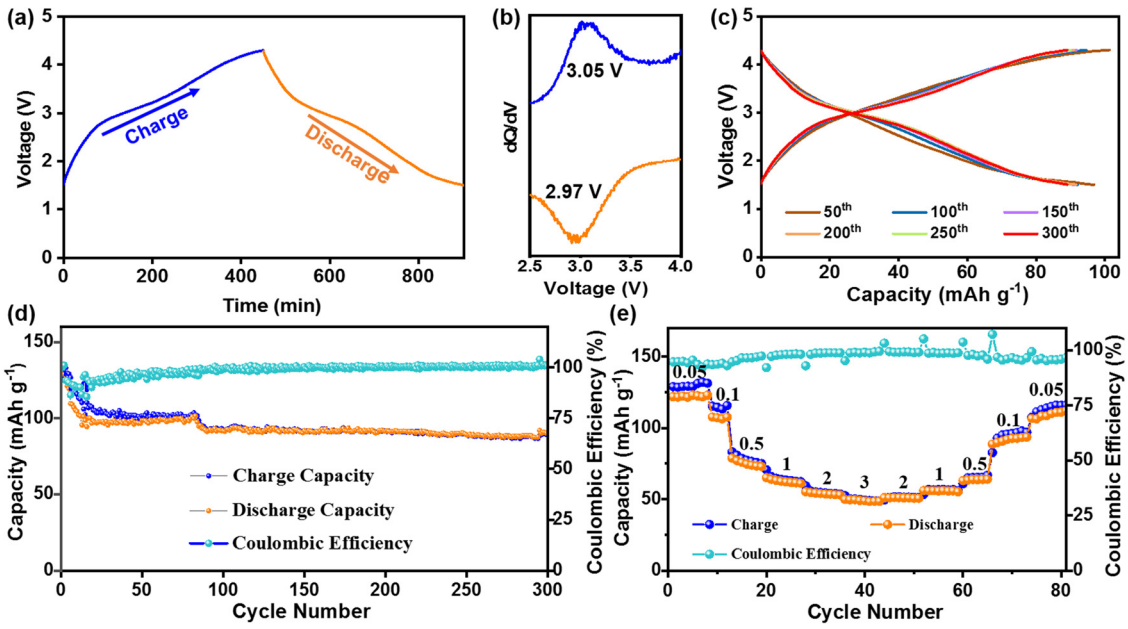

FIG. 2. Electrochemical reversibility of Na^+ de-/intercalation in Na_2FeF_4 in the voltage window of 1.5–4.3 V. (a) Representative charge/discharge curve at 0.1 C. (b) The corresponding dQ/dV vs voltage curve. (c)–(e) Long-term cycling stability test at 0.1 C; (c) the evolution of charge/discharge curves; (d) capacity and CE evolution; (e) rate performance from 0.05 to 3 C.

despite the different capacity (Fig. S7 in the supplementary material). Both cases shall be working on the Li^+ de-/intercalation reaction by comparing with Na-based half cells.

To investigate the electrochemical reaction mechanism, Fe *K*-edge synchrotron x-ray absorption spectroscopies (XAS) were recorded, which revealed that the reversible capacity is mainly attributed to the Fe^{2+}/Fe^{3+} redox couple. In detail, by comparing the Fe *K*-edge x-ray absorption near-edge spectra (XANES) [Fig. 3(a)], it is seen that a shift of the main-edge toward higher energy was detected in the 4.3 V-charged sample, indicating the oxidization of the Fe atom during the charging process. Meanwhile, an opposite shift was observed in the 1.5 V-discharged sample, suggesting the reduction of the Fe atom during the discharging process.[11,12] XANES curves of 1.5 V-discharged and pristine samples are highly overlapped, revealing the good reversibility of the process. Such evolution confirmed that the redox activity of Na_2FeF_4 in the voltage window of 1.5–4.3 V is based on the Fe^{2+}/Fe^{3+} redox couple.

In addition, the Fe extended x-ray absorption fine structure (EXAFS) of Na_2FeF_4 samples in different states was examined. As shown in Fig. 3(b), the k^3-weighted R-space EXAFS patterns displayed similar profiles of a strong peak centering around 1.5 Å, suggesting that the Na^+ de-/intercalation had not triggered serious damage to the environment of the central Fe atom, and its nearest shells were mostly maintained. This indicated the stability of the FeF_6 coordination environment to some extent, since it withstood the structural and charge perturbation caused by charging and discharging. Meanwhile, the Fe–F peaks shift to smaller and larger radius for the charged and discharged states, respectively. Such evolution is in agreement with the bonding trend of Fe^{3+}–F and Fe^{2+}–F and, therefore, further demonstrates the reversibility of the redox reactions of Fe^{2+}/Fe^{3+} in the 1.5–4.3 V voltage range.

The structural evolution was also monitored by collecting PXRD patterns on recovered samples. As shown in Fig. 3(c), the diffraction peak at 18.3° is related to the (011) plane of Na_2FeF_4, and the peaks at

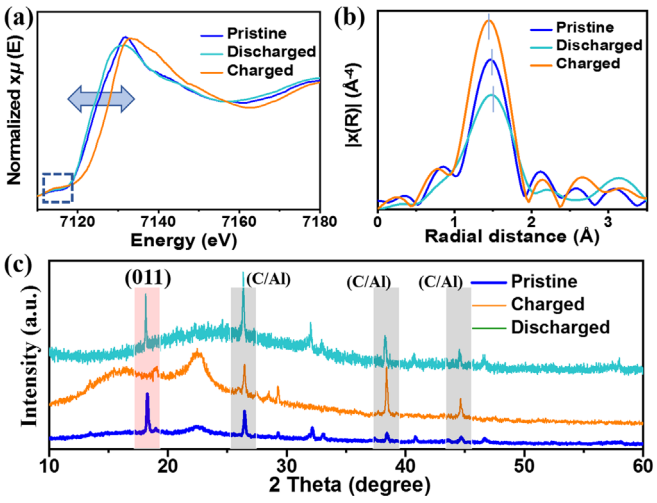

FIG. 3. Electrochemical reaction mechanism study of Na_2FeF_4 in the voltage window of 1.5–4.3 V. (a), normalized Fe *K*-edge XANES spectra of samples at pristine, 4.3 V-charged, and 1.5 V-discharged state. (b) The corresponding R-space EXAFS. (c) *Ex situ* PXRD patterns.

26.3°, 38.3°, and 44.6° come from the current collector. At the charged state, PXRD shows an essentially amorphous material with the weakened (011) peak shifting to higher angle (19.0°), while at the discharged state, the crystallinity of the original phase is recovered and the diffraction peak of the (011) plane returns back to lower angle. It is unfortunate that the precise determination of the structural changes upon cycling by lab-based PXRD is not possible. On the one hand, the crystallites had been sized-down to sub-micrometers and mixed with conductive carbon and binder before constructing into cells. On the other hand, the activating process has probably formed a cathode–electrolyte interface covering the cathode, and the electrochemical grinding effect further reduced the crystallinity of Na_2FeF_4 particles. To make the situation worse, the only available Cu Kα-based PXRD facility during this study induced strong fluorescence effects on our Fe-contained sample and lowered resolution of the PXRD patterns.

Finally, we carried out first-principles calculations based on a hybrid density-functional theory/Hartree–Fock approach[28] to further elucidate the electrochemical activity mechanism. The iron ion in Na_2FeF_4 is found to be stable as high-spin Fe^{2+} with a calculated magnetic moment of 3.73 μ_B. The compound has a calculated bandgap of 3.5 eV (indirect), and the top of the valence band is predominantly composed of Fe 3*d* states (Fig. S8 in the supplementary material). As Na extraction involves removing electrons from the valence-band top, the electronic structure suggests that the intrinsic extraction/(re)insertion would involve the Fe^{2+}/Fe^{3+} redox center. Indeed, we find that Fe^{2+} is oxidized to Fe^{3+} upon removing the first Na from Na_2FeF_4; the calculated magnetic moment of high-spin Fe^{3+} is 4.35μ_B. The average redox potential is 3.03 V vs Na between Na_2FeF_4 and $NaFeF_4$ in excellent agreement with the experimental value. Further removal of Na from $NaFeF_4$ results in Fe^{3+} being oxidized to Fe^{4+}; however, this redox reaction has a very high voltage (6.58 V vs Na) and, thus, could not be observed in the experiments.

In summary, an iron-based fluoride, Na_2FeF_4, has been developed by a mild hydrothermal reaction, and its electrochemical activity for sodium-ion storage has been investigated. Its structure contains a framework of parallel-aligned $[FeF_4]_\infty$ chains with Na^+ ions locating between the chains. When cycling in the window of 1.5–4.3 V against Na^+/Na, Na_2FeF_4 is capable of reversibly delivering a capacity of ~90 mAh g^{-1} for 300 cycles with redox reactions at ~3.0 V. Such an activity is based on Na^+ de-/insertion upon Fe^{2+}/Fe^{3+} reactions, as illustrated by synchrotron XAS, PXRD, and first-principles calculations. The present study offers an effective preparation method of a Fe^{2+}-based fluoride, using oxalate as the Fe^{2+} valence state protector, and provides a fluoride cathode for sodium-ion storage.

See the supplementary material for details on the experiments and calculations, crystallographic data, SEM and EDS, IR, air stability, electronic structure, and Li-half cell performance.

The authors gratefully acknowledge the financial support from the National Natural Science Foundation of China (Nos. 52125105, 22005329, and 51972329), the NSFC/RGC Joint Research Scheme (Nos. 52061160484 and N_CityU104/20), the Shenzhen International Collaboration Research Project (No. GJHZ20210705141407023), the Shenzhen Science and Technology Planning Project (Nos. JCYJ20190807172001755 and JCYJ20200109115624923), and the Science and Technology Planning Project of Guangdong Province

(Nos. 2019A1515110975, 2021A1515010184, and 2019TX05L389). The calculations were carried out using resources of the Center for Computationally Assisted Science and Technology (CCAST) at North Dakota State University, which were made possible in part by NSF MRI Award No. 2019077. Sincere thanks to Dr. Yongping Zheng for helpful discussion.

AUTHOR DECLARATIONS

Conflict of Interest

The authors have no conflicts to disclose.

Author Contributions

Q.Y. and H.X. performed sample preparation, characterizations and cell construction. K.H. conducted simulations. X.Z. and P.K. recorded synchrotron XAS data. W.Y. conceived the idea. P.L. and Y.T. supervised the project. All the authors discussed the results and commented on the manuscript.

Qi Yan: Writing – original draft (equal). **Huan Xu:** Writing – original draft (supporting). **Khang Hoang:** Writing – review & editing (supporting). **Xiaolong Zhou:** Writing – original draft (supporting). **Pinit Kidkhunthod:** Writing – review & editing (supporting). **Phil Lightfoot:** Writing – review & editing (equal). **Wenjiao Yao:** Writing – review & editing (equal). **Yongbing Tang:** Writing – review & editing (equal).

DATA AVAILABILITY

The data that support the findings of this study are available from the corresponding authors upon reasonable request.

REFERENCES

[1]S. Y. Liu, M. Sun, S. Zhang, S. Liu, D. J. Li, Z. Niu, Y. Li, and S. Wang, Appl. Phys. Lett. **118**, 141903 (2021).
[2]Y. Yang, H. Zhang, S. Hou, T. Wang, W. Chen, S. Xian, Z. Zhang, and Y. Mao, Appl. Phys. Lett. **119**, 161106 (2021).
[3]F. L. M. Bernal, B. Gonano, F. Lundvall, D. S. Wragg, H. Fjellvåg, F. Veillon, W. A. Sławiński, and Ø. S. Fjellvåg, Phys. Rev. Mater. **4**, 114412 (2020).
[4]R. M. Dubrovin, L. N. Alyabyeva, N. V. Siverin, B. P. Gorshunov, N. N. Novikova, K. N. Boldyrev, and R. V. Pisarev, Phys. Rev. B **101**, 180403 (2020).
[5]M. Leblanc, V. Maisonneuve, and A. Tressaud, Chem. Rev. **115**, 1191 (2015).
[6]Y. Li, Y. Lu, P. Adelhelm, M. M. Titirici, and Y. S. Hu, Chem. Soc. Rev. **48**, 4655 (2019).
[7]Q. Liu, Z. Hu, M. Chen, C. Zou, H. Jin, S. Wang, S. L. Chou, and S. X. Dou, Small **15**, 1805381 (2019).
[8]X. Xiang, K. Zhang, and J. Chen, Adv. Mater. **27**, 5343 (2015).
[9]F. Lv, Y. Zhang, M. Wu, and Y. Gu, Appl. Phys. Lett. **119**, 023903 (2021).
[10]B. Ji, W. Yao, Y. Zheng, P. Kidkhunthod, X. Zhou, S. Tunmee, S. Sattayaporn, H. M. Cheng, H. He, and Y. Tang, Nat. Commun. **11**, 1225 (2020).
[11]T. Song, W. Yao, P. Kiadkhunthod, Y. Zheng, N. Wu, X. Zhou, S. Tunmee, S. Sattayaporn, and Y. Tang, Angew. Chem., Int. Ed. Engl. **59**, 740 (2020).
[12]W. Yao, A. R. Armstrong, X. Zhou, M. T. Sougrati, P. Kidkhunthod, S. Tunmee, C. Sun, S. Sattayaporn, P. Lightfoot, B. Ji, C. Jiang, N. Wu, Y. Tang, and H. M. Cheng, Nat. Commun. **10**, 3483 (2019).
[13]K. V. Kravchyk, T. Zünd, M. Wörle, M. V. Kovalenko, and M. I. Bodnarchuk, Chem. Mater. **30**, 1825 (2018).
[14]A. Kitajou, H. Komatsu, K. Chihara, I. D. Gocheva, S. Okada, and J. i Yamaki, J. Power Sources **198**, 389 (2012).
[15]U. K. Dey, N. Barman, S. Ghosh, S. Sarkar, S. C. Peter, and P. Senguttuvan, Chem. Mater. **31**, 295 (2019).
[16]H. Park, Y. Lee, M-k Cho, J. Kang, W. Ko, Y. H. Jung, T.-Y. Jeon, J. Hong, H. Kim, S. T. Myung, and J. Kim, Energy Environ. Sci. **14**, 1469 (2021).
[17]W. Liu, W. Wang, M. Qin, and B. Shen, Ceram. Int. **46**, 11436 (2020).
[18]A. Le Baila and A. M. Mercier, Powder Diffr. **18**, 128 (2003).
[19]R. A. Shakoor, S. Y. Lim, H. Kim, K. W. Nam, J. K. Kang, K. Kang, and J. W. Choi, Solid State Ion. **218**, 35 (2012).
[20]H. He, W. Yao, S. Tunmee, X. Zhou, B. Ji, N. Wu, T. Song, P. Kidkhunthod, and Y. Tang, J. Mater. Chem. A **8**, 9128 (2020).
[21]W. Wang, B. Ji, W. Yao, X. Zhang, Y. Zheng, X. Zhou, P. Kidkhunthod, H. He, and Y. Tang, Sci. China Mater. **64**, 1047 (2021).
[22]S. I. Akimoto, Phys. Earth Planet Inter. **3**, 189 (1970).
[23]R. Kanno, Y. Takeda, K. Murata, and O. Yamaoto, Solid State Ion. **39**, 233 (1990).
[24]D. Kurzydłowski, M. Derzsi, A. Budzianowski, Z. Jagličić, W. Koźmiński, Z. Mazej, and W. Grochala, Eur. J. Inorg. Chem. **2010**, 2919.
[25]I. Plitz, F. Badway, J. Al-Sharab, A. DuPasquier, F. Cosandey, and G. G. Amatucci, J. Electrochem. Soc. **152**, A307 (2005).
[26]Q. Tian, J. Alloys Compd. **699**, 540–547 (2017).
[27]N. Wu, Y.-J. Yang, T. Jia, T.-H. Li, F. Li, and Z. Wang, J. Mater. Sci. **55**(14), 6030–6036 (2020).
[28]J. Heyd, G. E. Scuseria, and M. Ernzerhof, J. Chem. Phys. **118**, 8207 (2003).